Inorganic Chemistry

Article

pubs.acs.org/IC

Studies of the Pathways Open to Copper Water Oxidation Catalysts Containing Proximal Hydroxy Groups During Basic Electrocatalysis

Deidra L. Gerlach,[†,∥] Salome Bhagan,[†,∥] Alex A. Cruce,[†] Dalton B. Burks,[†] Ismael Nieto,[‡] Hai T. Truong,[‡] Steven P. Kelley,[†] Corey J. Herbst-Gervasoni,[‡] Katherine L. Jernigan,[†] Michael K. Bowman,[†] Shanlin Pan,[†] Matthias Zeller,[§] and Elizabeth T. Papish*[,†]

[†]Department of Chemistry, The University of Alabama, Box 870336, Tuscaloosa, Alabama 35487-0336, United States

[‡]Department of Chemistry, Drexel University, 3141 Chestnut Street, Philadelphia, Pennsylvania 19104, United States

[§]Department of Chemistry, Youngstown State University, One University Plaza, Youngstown, Ohio 44555, United States

Supporting Information

ABSTRACT: Water oxidation can lead to a sustainable source of energy, but for water oxidation catalysts to be economical they must use earth abundant metals. We report here 2:1 6,6′-dihydroxybipyridine (6,6′-dhbp)/copper complexes that are capable of electrocatalytic water oxidation in aqueous base (pH = 10−14). Two crystal structures of the complex that contains 6,6′-dhbp and copper(II) in a ratio of 2:1 (complex **1**) are presented at different protonation states. The thermodynamic acid dissociation constants were measured for complex **1**, and these show that the complex is fully deprotonated above pH = 8.3 (i.e., under water oxidation conditions). CW-EPR, ENDOR, and HYSCORE spectroscopy confirmed that the 6,6′-dhbp ligand is bound to the copper ion over a wide pH range which shows how pH influences precatalyst structure. Additional copper(II) complexes were synthesized from the ligands 4,4′-dhbp (complex **2**) and 6,6′-dimethoxybipyridine (complexes **3** and **4**). A zinc complex of 6,6′-dhbp was also synthesized (complex **5**). Crystal structures are reported for **1** (in two protonation states), **3**, **4**, and **5**. Water oxidation studies using several of the above compounds (**1**, **2**, **4**, and **5**) at pH = 12.6 have illustrated that both copper and proximal OH groups are necessary for water oxidation at a low overpotential. Our most active catalyst **1** was found to have an overpotential of 477 mV for water oxidation at a moderate rate of k_{cat} = 0.356 s^{-1} with a competing irreversible oxidation event at a rate of 1.082 s^{-1}. Furthermore, our combined work supports previous observations in which OH/O^- groups on the bipyridine rings can hydrogen bond with metal bound substrate, support unusual binding modes, and potentially facilitate proton coupled electron transfer.

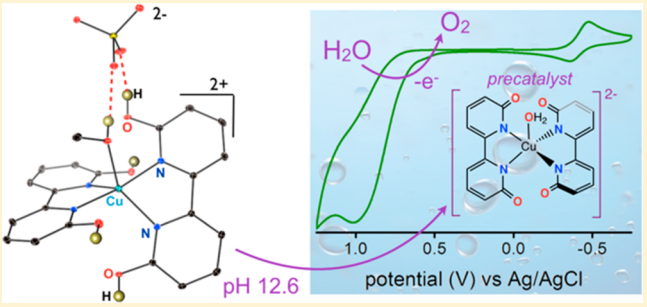

INTRODUCTION

A sustainable energy economy (eqs 1−3) is attainable by mimicking the catalytic efficiency of the oxygen evolving complex in photosystem II (PS II).[1] The active site of the oxygen evolving complex in PS II contains hydrogen bonding residues near its Mn_4Ca cluster which plays a role in proton shuttling to facilitate the kinetically challenging water oxidation reaction (eq 1).[2,3]

$$2H_2O \rightarrow O_2 + 4H^+ + 4e^- \quad (1)$$

$$4H^+ + 4e^- \rightarrow 2H_2 \quad (2)$$

$$2H_2O \rightarrow O_2 + 2H_2 \quad (3)$$

Significant developments utilizing metals such as Ru,[4] Ir,[5,6] Mn,[7] Fe,[8] Co,[9,10] Ni,[11] and Cu[12−15] as water oxidation catalysts (WOCs) have been reported. However, water oxidation catalysts with low overpotentials remain elusive and are a major goal of contemporary research. Lower overpotentials can be achieved by catalysts that facilitate proton coupled electron transfer (PCET) and stabilize key intermediates.[4,16] We postulated that the recently designed ligand, 6,6′-dihydroxybipyridine (6,6′-dhbp),[17−20] could perform both of these functions with copper, and the results to support this hypothesis are described herein.

Previously, we reported iridium water oxidation catalysts featuring 6,6′-dihydroxybipyridine (6,6′-dhbp) and 4,4′-dhbp ligands. These catalysts show that initial rates of water oxidation can be increased by a factor of ∼100 simply by changing pH from 3 to 6.[21] Our studies demonstrated that enhanced rates for water oxidation catalysis are due to ligand deprotonation which facilitates metal complex oxidation.[21] Parallel water oxidation studies with ruthenium complexes of 6,6′-dhbp and 6,6′-dimethoxybipyridine (6,6′-dmbp) have illustrated that methoxy and hydroxy groups near the metal form hydrogen bonds (including with Ru bound aqua substrate) and such interactions may stabilize reactive intermediates.[22] Thus, 6,6′-

Received: May 1, 2014
Published: November 26, 2014

   dx.doi.org/10.1021/ic501018a | *Inorg. Chem.* 2014, 53, 12689−12698

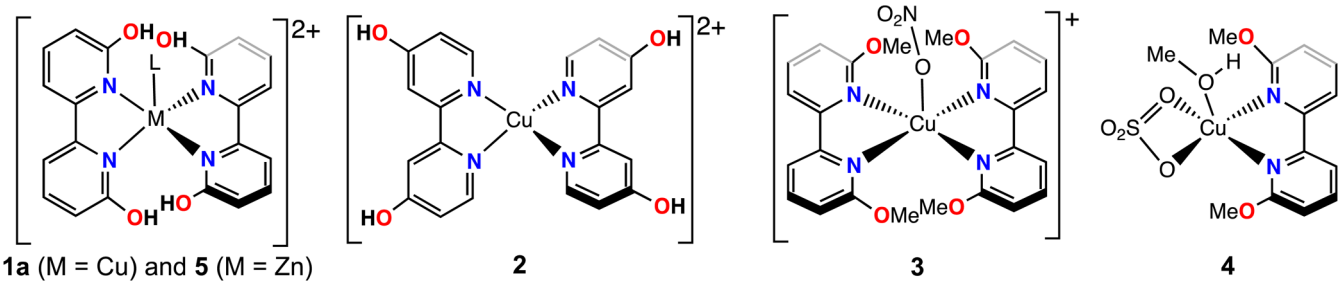

Figure 1. Structural diversity of complexes (**1**–**5**) prepared for this study.

dhbp ligands have interesting, pH sensitive properties,[18,23] and our group and others have shown that metal complexes thereof catalyze several different types of reactions,[17,19,20] including both oxidative[24] and reductive[18,25] processes.

We now extend the study of dihydroxy- and dimethoxybipyridine ligand series to copper(II) complexes. Recently, others have shown that *in situ* prepared 1:1 mixtures of copper(II) salts and 6,6′-dhbp ligands form a coordination polymer in the crystal phase and exhibit electrocatalytic water oxidation.[26] In our study, monomeric copper(II) complexes exhibiting primarily 2:1 ligand to metal ratios are investigated as water oxidation catalysts. Equilibrium constants are determined for deprotonation events and provide insight into catalytically relevant changes at the metal center. ENDOR and HYSCORE spectroscopy herein demonstrate the continuous ligation of the 6,6′-dhbp ligand to the copper(II) ion through the pH range where water oxidation is tested. The activity of catalysts containing hydrogen bonding OH/O^- groups near and far from the metal center (in 4,4′-dhbp and 6,6′-dhbp) and hydrogen bond accepting methoxy groups (in 6,6′-dmbp) is investigated.

RESULTS

Inspired by copper WOCs using bipy ligands,[12] we synthesized a series of copper(II) complexes using 6,6′-dhbp and closely related derivatives, shown schematically in Figure 1 with noncoordinating anions omitted. Monomeric copper–ligand complexes were formed from copper(II) nitrate (**3**) and copper(II) sulfate (**1**, **2**, **4**) to demonstrate the significant influence of varying anions and solvents. Additionally, a well-characterized monomeric zinc analogue was prepared as a control (**5**). Metal to ligand ratios are 1:1 in **4** and 1:2 in **1**, **2**, **3**, and **5**. Structural diversity in the array of dxbp (x = hydroxy or methoxy) derived divalent copper and zinc complexes are first discussed, and subsequently thermodynamic acidities and water oxidation studies on selected compounds are described.

Synthesis and Structural Studies. *Reaction of 2 equiv 6,6′-dhbp + $CuSO_4$ Leads to* ***1****.* Treating copper(II) sulfate with 6,6′-dhbp in ethylene glycol resulted in the clean formation of complexes with a 2:1 ratio of ligand to metal which were fully characterized (see Experimental Section and Supporting Information). Two different protonation states of $[(6,6'\text{-dhbp})_2Cu]^{n+}$ (**1**) were obtained as brown crystals and green crystals, from a single sample by slow evaporation from methanol. X-ray crystallography was used to identify the brown crystals as the fully protonated, pentacoordinate copper bis(6,6′-dhbp) methanol sulfate salt, $[(6,6'\text{-}(OH)_2\text{-bpy})_2Cu(CH_3OH)]SO_4$ (**1a**), Figure 2. The green crystals were identified as doubly deprotonated tetracoordinate copper bis(6,6′-dhbp) $[(6\text{-OH-}6'\text{-O-bpy})_2Cu]\cdot(CH_3OH)_2$ (**1c**), Figure 3. Complexes **1a**, **1c**, and the other protonation states for **1** (**1b**, **1d** (not observed), **1e**) are shown in Scheme 1.

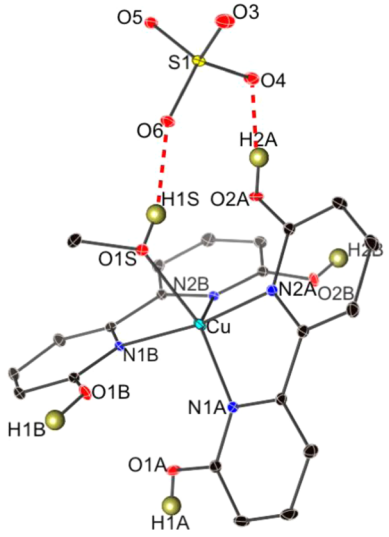

Figure 2. Structural diagram of the fully protonated complex, $[(6,6'\text{-dhbp})_2Cu(CH_3OH)]SO_4$ (**1a**). This complex features OH to sulfate hydrogen bonds, as shown as red dashed lines. Non-hydrogen atom ellipsoids are shown at 30% probability. Hydrogen atoms are shown as spheres of arbitrary radius. Most hydrogen atoms are omitted for clarity.

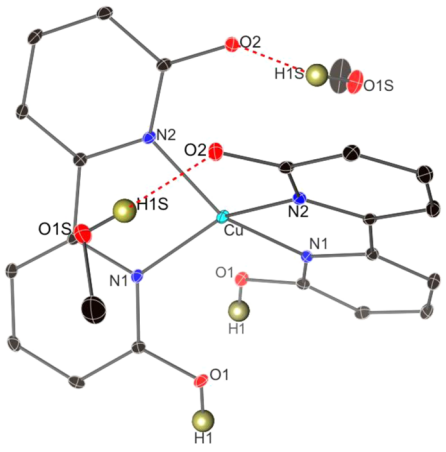

Figure 3. Structural diagram of the doubly deprotonated complex, $[(6\text{-OH-}6'\text{-O-bpy})_2Cu]\cdot(CH_3OH)_2$ (**1c**). This complex features O^- to methanol hydrogen bonds, as shown with red dashed lines. Non-hydrogen atom ellipsoids are shown at 30% probability. Hydrogen atoms are shown as spheres of arbitrary radius. Most hydrogen atoms are omitted for clarity.

dx.doi.org/10.1021/ic501018a | *Inorg. Chem.* 2014, 53, 12689–12698

Scheme 1. Complex Hydrogen Ion Interrelationships of $[(6,6'\text{-dhbp})_2Cu]^n$ (Where n = Charge) Complexes (1) in Water (L = Solvent)

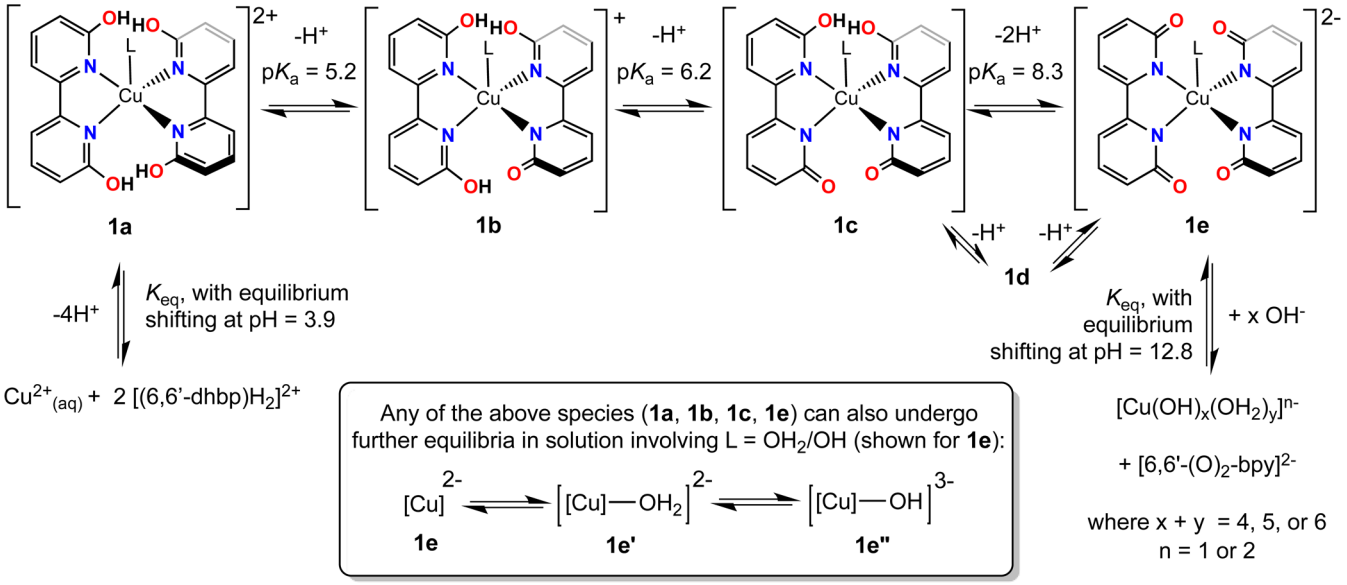

Complex **1a** (Figure 2) features a distorted trigonal bipyramidal copper center with τ = 0.697.[27] The coordinated methanol has a Cu−O bond distance of 2.340 Å, and the 6,6′-dhbp ligands approach the metal more closely (Cu−N distances ∼1.96−2.07 Å). Both the bound methanol and the OH groups of all the 6,6′-dhbp ligands are hydrogen bond donors to nearby sulfate counteranions (O···O distances range from ∼2.54 to 2.78 Å indicating hydrogen bonds). The crystal packing reveals that the copper complex cations are arranged into sheets divided by interwoven planes of the sulfate anions. Interestingly, π stacking occurs between the 6,6′-dhbp ligands of two molecules opposite an inversion center.

Doubly deprotonated **1c** (Figure 3) features a distorted geometry around copper that is intermediate between tetrahedral and square planar. The twist angles between planes that contain each 6,6′-dhbp ligand range from 52° to 55°. The Cu−N bonds are slightly shortened (relative to **1a**), and all are around ∼1.97 Å. This reflects the negative charge on each ligand and the resulting partial negative charge on N due to resonance. Consistent with this explanation is a slightly decreased C−O distance[28] due to double bond character (1.290(3) vs 1.320(3) Å). Note that each dhbp ligand has one deprotonated and one protonated oxygen. Two crystallographically distinct methanol molecules are hydrogen bonded to the 6,6′-dhbp ligand in the crystal phase, but notably they do not coordinate. Hydrogen bonds exist between OH and O^- of the dhbp ligands (O2···O1 = 2.488(2) Å) in neighboring molecules in the packing diagram (not shown in Figure 3). Also, there are moderate strength hydrogen bonds from O^- of dhbp to methanol (O2···O1S = 2.713(3) Å). An infinite head-to-tail chain of molecules along the crystallographic b axis results from this hydrogen bonding, as described further in the Supporting Information. Although the coordination number differs between these two structures of the crystallized complex **1** in two protonation states, both metal centers have the capacity for further ligation in the presence of coordinating solvent. Spacefill models of each structure show the copper(II) ion as being accessible to a sixth ligand or fifth ligand for complexes **1a** and **1c**, respectively.

Reaction of 2 equiv 4,4′-dhbp + $CuSO_4$ Leads to ***2****.* Complex **2** was prepared in a manner analogous to **1** by using 4,4′-dhbp and copper sulfate in a 2:1 ratio. Complex **2** was synthesized to investigate the role of hydroxyl groups far from the copper metal center for water oxidation studies. The light blue solid was obtained in 82% yield and characterized by UV−vis and IR spectroscopy and elemental analysis (see Experimental Section and Supporting Information). Crystals suitable for X-ray diffraction were not obtained despite several attempts, but complex **2** is likely to have a coordination geometry similar to that of complex **1a** where the possibility of coordination of a fifth ligand L (H_2O or MeOH) is possible in solution.

Reaction of 6,6′-dmbp + Cu(II) Leads to ***3*** *or* ***4*** *Depending on Whether $Cu(NO_3)_2$ or $CuSO_4$ Is Used.* Complex **3** was formed from the reaction of 6,6′-dmbp and $Cu(NO_3)_2{\cdot}2.5H_2O$ (Figure 4). The formula unit obtained by crystallography was $[(6,6'\text{-dmbp})_2Cu(NO_3)]_2[Cu(NO_3)_4]$ wherein both copper ions are divalent (see Supporting Information). This structure features a five-coordinate trigonal bipyramidal copper(II) ion ligated by two (*N,N*) bound 6,6′-dmbp ligands and one κ^1-nitrate ligand with τ = 0.803. The Cu(II) ion in $[Cu(NO_3)_4]^{2-}$

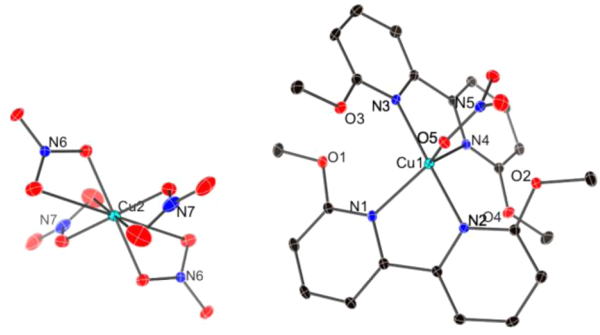

Figure 4. Copper(II) complex of 6,6′-dimethoxybipyridine (**3**) with the formula unit $[(6,6'\text{-dmbp})_2Cu(NO_3)]_2[Cu(NO_3)_4]$. Ellipsoids are shown at 30% probability. Hydrogen atoms are omitted for clarity, and only one $[(6,6'\text{-dmbp})_2Cu(NO_3)]$ unit is shown.

dx.doi.org/10.1021/ic501018a | *Inorg. Chem.* 2014, 53, 12689−12698

binds each nitrate in an asymmetric κ^2 mode with four short Cu−O bonds and four long Cu−O bonds. This anion is rare but has been observed in seven crystal structures in the Cambridge Structural Database.[29,30] However, the poor solubility of this complex (**3**) in basic aqueous solution combined with the presence of two distinct copper environments made this species unsuitable for catalytic water oxidation studies.

In contrast, the reaction of 6,6′-dmbp with copper(II) sulfate using a 2-fold excess of the dmbp ligand resulted in isolation of a monomeric copper complex (**4**, Figure 5) with a 1:1 ligand to

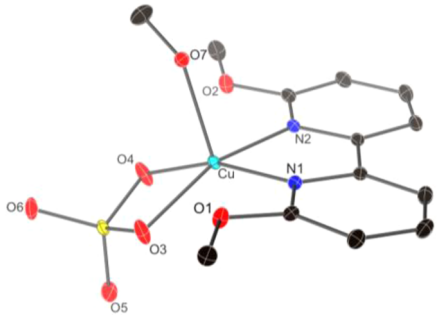

Figure 5. Structural diagram of [(6,6′-dmbp)Cu(SO_4)(CH_3OH)] (**4**). This complex features OH of methanol to sulfate hydrogen bonds (not shown), involving neighboring molecules. Ellipsoids are shown at 30% probability. All hydrogen atoms are omitted for clarity.

metal ratio. Complex **4** [(6,6′-dmbp)Cu(SO_4)(CH_3OH)] was isolated in 75% yield by recrystallization from methanol and exhibits a square pyramidal geometry around Cu (τ = 0.075) with an apical methanol molecule. Hydrogen bonds between coordinated methanol and neighboring sulfate groups (O5···O7 = 2.671(2) Å) extend along the *a* direction of the unit cell and connect the molecules in a two-dimensional network.

Reaction of 6,6′-dhbp + $Zn(ClO_4)_2$ Leads to ***5****.* A zinc complex of 6,6′-dhbp was prepared to determine whether copper is essential for water oxidation (*vide infra*). Treatment of zinc(II) perchlorate hexahydrate with 6,6′-dhbp led to clean formation of [(6,6′-dhbp)$_2$Zn](ClO_4)$_2$ (**5**) in 29% yield after recrystallization from acetonitrile and hexane (3:1). The crystal structure (Figure 6) shows that the geometry around zinc is a nearly perfect tetrahedron (the torsion angle between the planes containing 6,6′-dhbp ligands is 87−88°), in contrast to the twisted alignment of ligands in **1c**. Hydrogen bonds are present between all OH groups of 6,6′-dhbp and neighboring disordered perchlorate anions (O···O hydrogen bonding distances range from 2.680(5) to 2.93(1) Å).

Protonation and Deprotonation States of Aqueous Species in Equilibrium. *Acid−Base Titrations of Complex* ***1*** *for Determining Protonation and Deprotonation States.* The two crystal structures afforded for complex **1** are snapshots of protonation/deprotonation states of this complex. The complex [(6,6′-dhbp)$_2$Cu(L)]SO_4 (**1**) contains four acidic hydrogens from four OH groups of the hydroxypyridine rings, Scheme 1. Further deprotonation events are possible for pentacoordinated complexes of **1** (L = aqua or methanol) as seen in the structure for complex **1a** where methanol is coordinated. The neutral, doubly deprotonated complex [(6-OH-6′-O-bpy)$_2$Cu] (**1c**) is tetracoordinate without methanol or water bound in the coordination sphere in the crystal phase (Figure 3). Deprotonation of 6,6′-dhbp results in an increase of negative

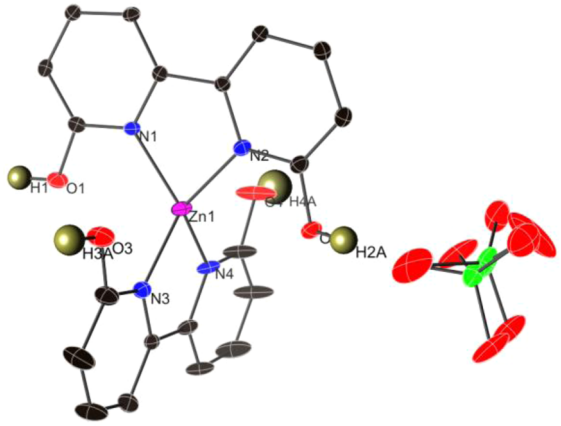

Figure 6. Structural diagram of [(6,6′-dhbp)$_2$Zn](ClO_4)$_2$·3CH_3CN (**5**). This complex features OH to O^- of perchlorate hydrogen bonds. The perchlorate anions are disordered in the crystal (Cl = green and O = red). Non-hydrogen atom ellipsoids are shown at 30% probability. Hydrogen atoms are shown as spheres of arbitrary radius. Most hydrogen atoms are omitted for clarity.

charge on the ligand and as a result binds more strongly to copper. Increasing the negative charge of the ligand supports lower coordination numbers on the metal center through resonance stabilized pyridinolate rings which delocalize the negative charge onto the nitrogen atoms.

Acid−base titrations were utilized to elucidate the pK_a values for the proposed species. UV absorption spectra recorded for **1** as a function of pH are shown in Figure 7 for the pH range 2.5−11, highlighting the most significant absorption features. Aqueous solutions of complex **1** (25 μM) at low pH have poor solubility and require the use of 0.013% ethylene glycol and 0.013% methanol as cosolvents in water. A plot of absorbance as a function of pH at λ = 369 nm is shown in Figure 7 (right) and has two inflection points at pH = 3.9 and 8.3. The region between pH 5 and 7 is not as well-defined by ∼0.5 pH unit increments for UV−vis absorbance measurements. Spectral studies were repeated utilizing increments of ∼0.1 pH units to better define this region, Figure 7 (right, inset). A plot of absorbance versus pH in the range pH = 5−6.5 results in the observation of two additional inflection points at pH values of 5.2 and 6.2. UV absorption spectra recorded for **1** as a function of pH are shown in Figure 8 for the pH range 9.3−13.4. A plot of the absorbance at 357 and 331 nm versus pH for the range 12.4−13.4 (see the Supporting Information) affords the elucidation of another inflection point at pH = 12.8. As described below, further experiments show that the inflection points at pH = 5.2, 6.2, and 8.3 are pK_a values for complex **1**, and the inflection points at 3.9 and 12.8 represent demetalation events occurring in the low and high pH regimes.

The pK_a values of 5.2 and 6.2 are each tentatively assigned to the removal of one proton from the 6,6′-dhbp ligands (Scheme 1, **1a** goes to **1b** goes to **1c**). Similarly, our studies of Ru^{II} and Ir^{III} complexes of 6,6′-dhbp showed pK_a values of 5−7.27 and 4.6, respectively,[18,21,23] for removal of ligand protons which are typically more acidic than protons of a metal-bound aqua ligand.[21,22] The last pK_a value (8.30) is tentatively assigned to the removal of 2 protons (Scheme 1, **1c** goes to **1e**, presumably via **1d**). This value is higher or similar to previously observed values for Ru^{II} complexes,[22,23] and this makes sense given the 2− charge associated with complete deprotonation of complex **1** to form **1e**. Deprotonation of Cu(II)-bound aqua ligands to

dx.doi.org/10.1021/ic501018a | *Inorg. Chem.* 2014, 53, 12689−12698

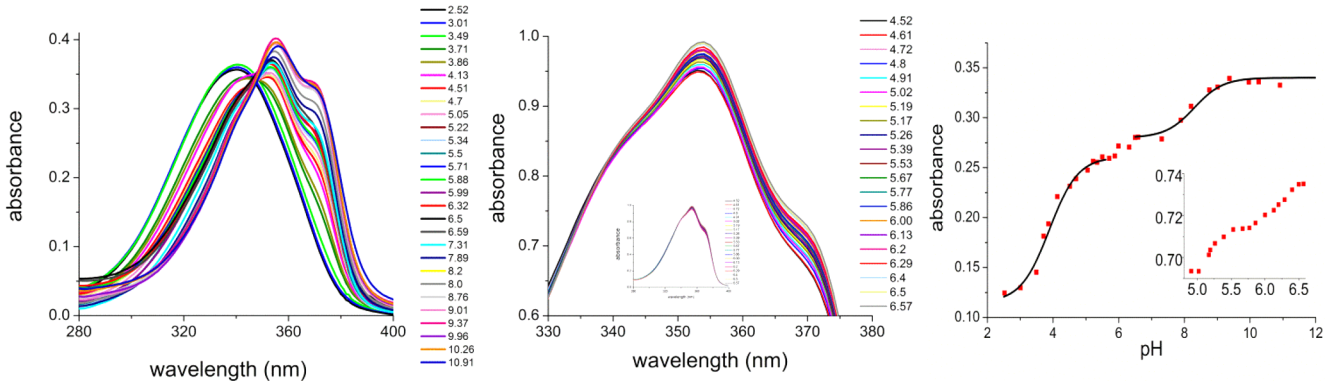

Figure 7. Left: UV−vis absorption spectra of aqueous solutions of $[(6,6'\text{-dhbp})_2Cu]SO_4$ (**1**) as a function of pH from pH = 2.5 to 11 at 25 °C. Middle: Same as left but from pH = 4.5 to 6.5 in 0.1 pH increments, and the inset shows the full peak shape. Right: Plot of absorbance (at λ = 369 nm) vs pH at 25 °C, and the inset shows the same plot from pH 5.0 to 6.5.

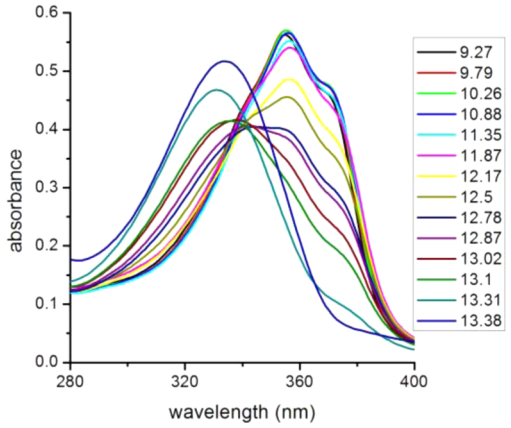

Figure 8. UV−vis absorption spectra of aqueous solutions of $[(6,6'\text{-dhbp})_2Cu]SO_4$ (**1**) as a function of pH from pH = 9.3 to 13.4 at 25 °C.

form hydroxide ligands is not supported by the HYSCORE evidence (below) until the high pH regime (pH > 12.8). Similarly, studies of Cu(II) bipyridine complexes have shown that the concentration of $[Cu(bpy)_2OH]^+$ does not predominate until pH 11.[31]

It should be noted that the absorption event that is most significant at 369 nm is primarily the $\pi-\pi^*$ of the aromatic dhbp ligand; thus, the largest change in absorption at this wavelength can be inferred to be a modification of the aromaticity of the ligand with likely minor to no change in absorbance for deprotonation of the possible fifth L ligand (H_2O or MeOH). The free 6,6′-dhbp ligand alone shows significant change in absorbance and the appearance of a distinct Gaussian signal in this region which can be described by loss of aromaticity (see the Supporting Information).

EPR studies on **1**, described below, show that significant changes in the coordination geometry (which could include fifth ligand L coordination of water or hydroxide) do not occur until above pH 10. As described below, the EPR data, in particular the HYSCORE, was instrumental in identifying that the low and high pH inflection points (pH = 3.9 and 12.8, respectively) are demetalation events for the 6,6′-dhbp ligand. Below pH = 3.9, the 6,6′-dhbp ligand is singly or doubly protonated (most likely), wherein the latter structure would have both oxygen and nitrogen atoms protonated and aromaticity is maintained. At this pH the copper ion will ligate six waters as in the known $[Cu(H_2O)_6]^{2+}$ complex. At pH above 12.8 the 6,6′-dhbp ligand is doubly deprotonated with two phenoxide groups. It is likely that the drive for demetalation of the 6,6′-dhbp ligand at high pH is due to hydroxide out-competing for coordination to the cupric ion.

The distribution of the species **1a**−**1e** has been plotted as a function of pH, as shown in Figure 9 (calculated from the pK_a

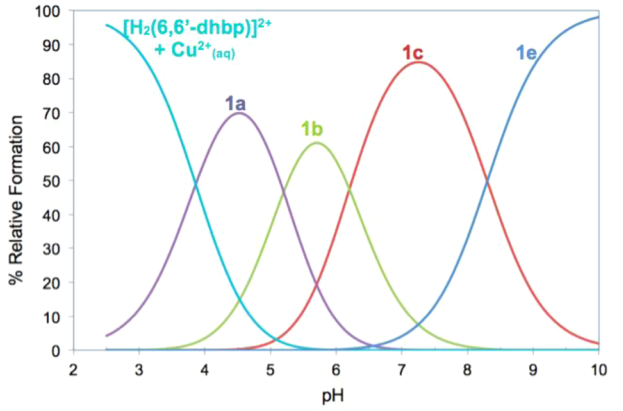

Figure 9. Calculated speciation diagram from pH 2.5 to 10 based upon the pK_a values for $[Cu(6,6'\text{-dhbp})_2]^{2+}$ (**1a**) and the EPR experiments.

values with Hyperquad Simulation and Speciation software). This shows that from pH 4.5 to 7 species **1a**, **1b**, and **1c** are all present simultaneously, and perhaps this explains the cocrystallization of **1a** and **1c**. Also, above pH 9 (i.e., water oxidation conditions, *vide infra*), species **1e** is dominant. Discussion of the speciation above pH 10 is in the EPR section below.

Similar acid−base titration studies of $[(4,4'\text{dhbp})_2Cu]^{2+}$ (**2**) by UV−vis absorption and potentiometric titrations were also performed, and two acid dissociation constants were observed in the range pH 5−8. Studies to assign acid dissociation constants using UV−vis spectral methods were inconclusive. Thus, exact pK_a values could not be obtained for **2**, see the Supporting Information. Similarly, potentiometric titration of the zinc complex **5** led to the observation of two pK_a values (tentatively, each may be the removal of two protons), but exact pK_a values could not be assigned (see the Supporting Information).

*CW-EPR, ENDOR, and HYSCORE Spectroscopy Were Used To Determine the Speciation of Complex **1** at Different pH*

dx.doi.org/10.1021/ic501018a | *Inorg. Chem.* 2014, 53, 12689−12698

Values. The continuous wave (CW) electron paramagnetic resonance (EPR) spectra (combined with electron nuclear double resonance (ENDOR) spectroscopy) can distinguish between N and O ligands on the copper, since hyperfine interactions of the N ligands produce broader resonances. The spectra show that the 6,6′-dhbp ligand(s) are bound to the metal ion throughout pH 5.7−12.6 (see the Supporting Information for CW-EPR spectra). This is a wide range that includes the majority of the deprotonation events observed by UV−vis absorption (*vide supra*) and the water oxidation conditions most extensively studied (*vide infra*). However, the 6,6′-dhbp ligand is not bound to Cu^{2+} at pH 3.5 and pH 13.3, and these spectra match those observed for $CuSO_4$ aqueous solutions prepared at the same pH values and correspond with previously noted demetalation events at low and high pH values (inflection points at pH = 3.9 and 12.8, respectively).

The CW spectra taken between pH values 5.7−10.0 are identical (species **A**), and thus, the acid dissociation constants (at pK_a = 5.2, 6.2, and 8.3) reported by UV−vis spectroscopy are indeed consistent with ligand deprotonation events. A substantial rearrangement at the metal center from pH 5 to 10 would lead to a major change in the EPR spectra. Thus, the data are not consistent with a fifth ligand, e.g., H_2O, coordinating to any significant extent in this pH regime.

As pH increases from pH 10 to 13.3, the EPR shows that, from pH 10 to ∼12, species **A** disappears and species **B** and **C** appear, but species **B** dominates the spectrum and species **C** is around 20% of the EPR spectrum from pH 11.5 to 12.6. Species **D** appears at pH 12, and the concentration steadily increases, ultimately becoming the lone species at pH 13.3, with the 6,6′-dhbp ligand completely dissociated (see speciation diagram in the Supporting Information). This transformation likely involves coordinating hydroxide ligands as the pH increases. The percentage of each species, *g*, and *A* values at each pH are shown in the Supporting Information. ENDOR spectroscopy (Supporting Information) further supports that the same number of 6,6′-dhbp ligands is bound to copper(II) at pH 8.2 and 11, but ligand loss occurs at pH 13.3.

While these EPR spectra do not account for the impact of oxidizing potentials on the complex geometry, at least it is clear that nitrogen ligands are present at pH 10−12.6 wherein water oxidation begins to occur at pH 11.5. At pH 12.6, which is the most frequently studied pH for water oxidation, the mixture is 36% species **B**, 23% species **C**, and 41% species **D** by simulating CW EPR. Thus, at pH 12.6, species **B** and **C** (together 59%) contain 6,6′-dhbp bound to Cu ion from the ENDOR data, but a significant portion of the sample has unligated copper. Spin quantification shows that no significant quantity of EPR silent material is present; thus, dinuclear copper species are unlikely in our precatalysts used for water oxidation. This helps to elucidate the nature of the species in solution during water oxidation in our studies (below) and perhaps present in other studies.[26]

Pulsed EPR was utilized to further identify species **A**, **B**, and **C**. Hyperfine selective correlation Spectroscopy (HYSCORE) is a pulsed EPR technique used to measure ENDOR frequencies, that is, NMR frequencies shifted by hyperfine interactions between the unpaired electron and nuclei near the copper center. HYSCORE gives a 2D representation of ENDOR frequencies similar to COSY in NMR. HYSCORE spectroscopy has been used to detect axial water protons and axial cysteine protons up to 0.3 nm away from the low-spin, active site heme of cytochrome P450.[32,33] HYSCORE can also detect ^{13}C up to 0.5 nm from the paramagnetic center.[34] Complex **1** has HYSCORE spectra showing protons from ligated water (pH 10−12.5), ^{13}C from 6,6′-dhbp ligands (pH 10−12.5), and hydroxide (pH 13.3).

HYSCORE spectra of complex **1**, up to at least pH = 11, have a distinct peak from ^{13}C along the diagonal near [4 MHz, 4 MHz]. Figure 10 shows the spectra at pH 11 for **1** compared

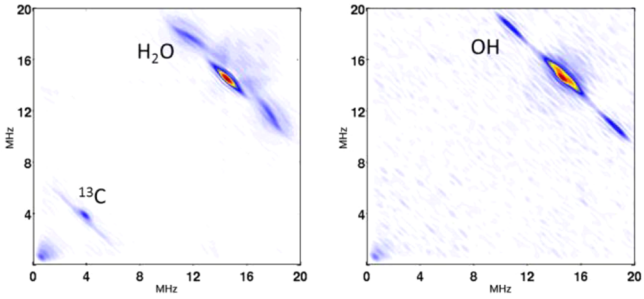

Figure 10. HYSCORE spectrum at pH 11 of (left) complex **1** and (right) $CuSO_4$ in 10% glycol. The intense peak near [14 MHz, 14 MHz] is from protons in solvent surrounding the complexes. The arcs flanking that peak near [18 MHz, 12 MHz] and [12 MHz, 18 MHz] are from protons on water (complex **1**) or hydroxide ($CuSO_4$) directly coordinated to the copper. Note the tilt of the signals from ligated water on complex **1** (also seen on $CuSO_4$ at low pH) compared to the straight lines from copper bound hydroxide in the frozen solution of $CuSO_4$ at high pH. The peak near [4 MHz, 4 MHz] is from natural abundance ^{13}C in the 6,6′-dhbp ligands.

to free $CuSO_4$ at the same pH with the same solvent conditions. There is a less intense streak running through the diagonal peak from ^{13}C having hyperfine couplings of as much as 6 MHz. This streak is caused by delocalization of the unpaired electron spin of the copper onto an aromatic ligand where the hyperfine couplings from natural abundance ^{13}C had a variety of values at the different carbons of the ligand. The full set of HYSCORE spectra is included in the Supporting Information.

The combined evidence includes the acid−base titrations interpreted by UV−vis spectroscopy and several EPR techniques for aqueous solutions of complex **1**. These experiments elucidate which species are present across a wide range of pH values, including typical water oxidation conditions. Scheme 1 depicts our interpretation of this data, including demetalation events as the pH is lowered below 3.9 and above 12.8. The species labeled as **A**, **B**, and **D** from the EPR data are assigned as **1e**, **1e**′ (**1e** with aqua ligand coordinated), and a copper hydroxide/aqua complex, respectively (Scheme 1). Species **C** is a minor component at all pH values so the assignment is uncertain, but it is likely to involve partial ligand loss to form a 1:1 complex of 6,6′-dhbp and Cu(II) with water or hydroxide completing the coordination sphere (the HYSCORE supports predominantly water coordination to Cu(II)).

Catalytic Water Oxidation Studies. Electrocatalytic studies of copper(II) complexes of 6,6′-dhbp (**1** added as **1a** and **1c**) and 4,4′-dhbp (**2**) were performed in solutions ranging in pH 10−14. Cyclic voltammetry (CV) experiments utilized 1 mM copper catalyst, 0.1 M NaOH/NaOAc aqueous electrolyte, glassy carbon working electrode (diameter 3 mm), Ag/AgCl reference electrode (with saturated KCl), and Pt counter electrode. Alkaline solutions of **1** showed irreversible and enhanced anodic current that indicates electrocatalytic water

dx.doi.org/10.1021/ic501018a | *Inorg. Chem.* 2014, 53, 12689−12698

oxidation at high pH values, as shown in Figure 11. Solutions of **1** used in this study were free from precipitate before potential

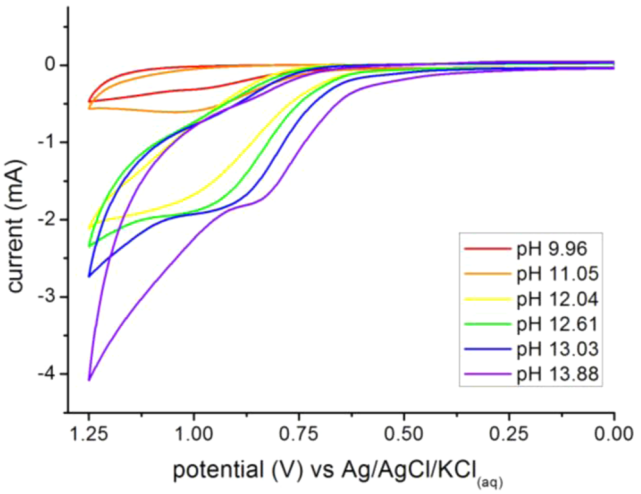

Figure 11. Cyclic voltammogram (CV) plots (non-background-corrected) of 1.0 mM $[(6,6'\text{-dhbp})_2Cu]SO_4$ (**1a**) as a function of pH on glassy carbon, scan rate = 100 mV/s in water with 0.1 M NaOAc/NaOH.

was applied. CV of complex **1** in dry propylene carbonate with increasing water additions showed no redox activity until alkali water (pH 12.6 with NaOH) was added to the system (see the Supporting Information). Water at high pH is therefore needed to activate the copper(II) complexes of 6,6′-dhbp in order to observe its redox activities and electrocatalytic water oxidation.

The scan rate dependence of CVs of 1.0 mM complex **1** at pH 12.6 in aqueous 0.1 M NaOAc/NaOH was obtained (Figure 12). At low potential the quasireversible reduction of $Cu^{II/I}$ is seen at −0.387 V (Figure 12). All CVs of complex **1** are fitted using digital simulation to illustrate its electrocatalytic activities as highlighted in Figure 13. Although the water oxidation of Cu complex involves multiple steps of proton coupled charge transfer steps,[4,13,14,35] the data fitting was done by assuming the Cu complex **1** undergoes a heterogeneous

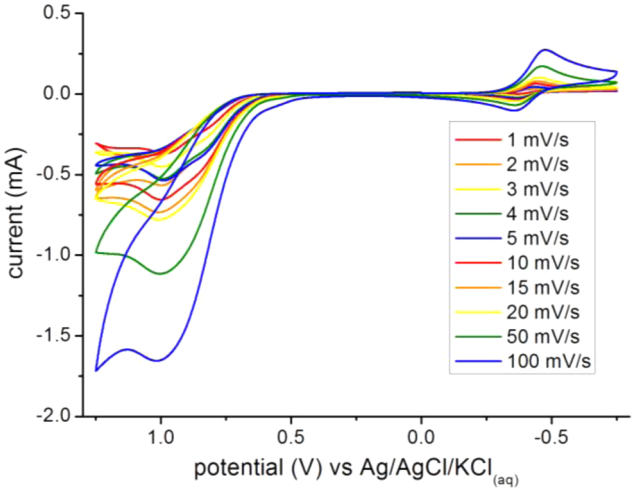

Figure 12. CV plots as a function of scan rate of for a 1.0 mM pH 12.6 solution of complex **1** on glassy carbon in water with 0.1 M NaOAc/NaOH, corrected for background (see Supporting Information for non-background-corrected and background scans).

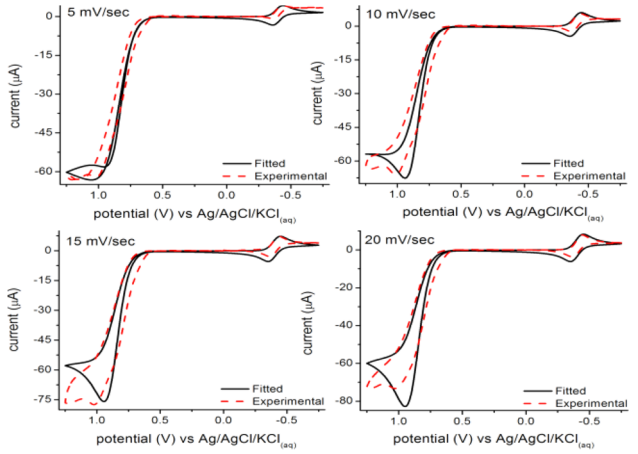

Figure 13. Simulated CVs of aqueous complex **1** at varied scan rate compared to experimental data (Figure 11) for the mechanistic fitting of the data.

charge transfer step through its aqua-coordinated product $[(6,6'\text{-}(O)_2\text{-bpy})_2Cu(H_2O)]^{2-}$, and two following homogeneous reactions, including one catalytic water oxidation and an irreversible reaction of the oxidized aqua-coordinated complex **1**. Such data fitting provides an estimate of the charge transfer rate and turnover frequency of the Cu complex, although the true mechanism needs further study to have an improved understanding. From the EPR and HYSCORE data for complex **1** at pH 12.6 it can be inferred that the major copper species present at this pH is the aqua-coordinated $[(6,6'\text{-}(O)_2\text{-bpy})_2Cu(H_2O)]^{2-}$ complex (species **B** or **1e′**). An initial oxidation of this complex occurs and is calculated with fitting to be at 0.766 V (vs Ag/AgCl). From this value the overpotential was calculated to be 477 mV. The subsequent water oxidation reaction occurs with an average turnover rate of 0.356 s^{-1}. We also found that an irreversible but noncatalytic pathway of the Cu complex competes with the water oxidation at a faster rate of 1.082 s^{-1}, forming some unidentified product (Scheme 2).

Scheme 2. Schematic View of the Fitted Water Oxidation Process Occurring in the Electrochemical Cell for Complex 1

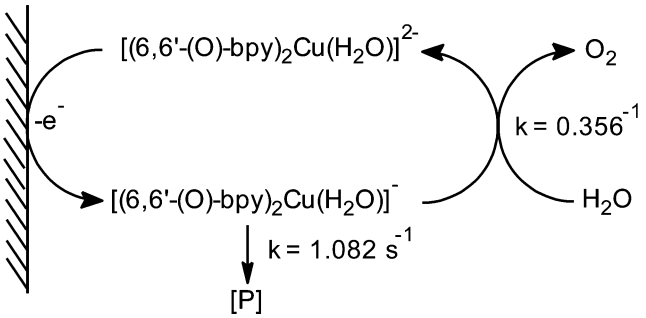

Bulk electrolysis of 1.0 mM of complex **1** at pH 12.6 in aqueous 0.1 M NaOAc at 0.9 V was carried out in an airtight cell in which the headspace of the vessel was sampled at regular intervals with a gastight syringe to be injected for manual sampling of the gas composition via GC−MS. An increase in the relative quantity of oxygen was observed indicating the accumulation of oxygen as positive potential was applied to complex **1** as was expected. Due to the sluggish rate of catalysis

dx.doi.org/10.1021/ic501018a | Inorg. Chem. 2014, 53, 12689−12698

by complex **1** to generate oxygen versus the rate of formation of an unknown inactive product the composition of oxygen was not expected to be and was not observed to be dramatic (see the Supporting Information).

Furthermore, the combined data support the catalysis (at pH 12.6) by a 6,6′-dhbp ligated copper complex like **1e**′ rather than simple copper salts (e.g., species **D**). Copper sulfate solutions at the same pH show no catalytic current. Also, in our study and another study,[26] both copper(II) and 6,6′-dhbp are necessary for water oxidation at pH 12.6. Other complexes including **4** and **5** (*vide infra*) and the 1:1 complexes of $CuSO_4$ and 4,4′dhbp and 4,4′-dmbp are inactive at water oxidation,[26] and this implies that the 6,6′-dhbp plays a role in water oxidation at pH 12.6.

For comparison, CV studies of complexes **1**−**5** were performed utilizing 1 mM of catalyst, 0.1 M NaOH/NaOAc pH 12.6 electrolyte, glassy carbon working electrode, Ag/AgCl reference electrode, and Pt counter electrode, Figure 14.

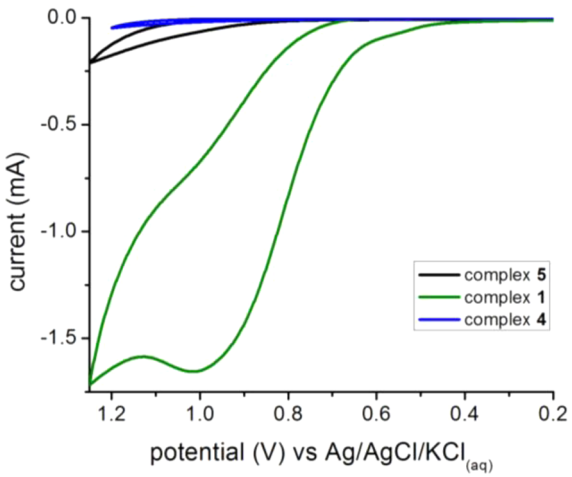

Figure 14. Comparison of 1 mM solution of complexes **1**, **4**, and **5** at pH 12.6 in 0.1 M NaOAc at glassy carbon electrode at a scan rate of 100 mV/s.

Solutions of $[(4,4'\text{-dhbp})_2Cu]^{2+}$ (**2**) did not exhibit any catalytic waves. Complex **3** precipitated when dissolved in electrolyte solution, and water oxidation studies were not performed. Similarly, complex **4** was also insoluble in electrolyte solution; however, water oxidation was attempted. A slightly larger current was obtained for **4** than for electrolyte alone (blank) without the observation of any catalytic waves. Complex **5** was fully soluble in pH 12.6 electrolyte, and a minor oxidative peak (Figure 14) was observed which is tentatively assigned to irreversible oxidation of the ligand in complex **5**, as is consistent with similar observations (at E = 1.16 V vs NHE) for a 1:1 mixture of Zn^{II} and 6,6′-dhbp.[26]

Complex **1** exhibits significantly lower TOF (at 0.356 s^{-1}) than other copper catalysts[12,14] but is similar to the value of 0.4 s^{-1} TOF reported for *in situ* prepared 1:1 Cu and 6,6′-dhbp complexes.[26] The overpotential observed (477 mV) for **1** places it at the low end of copper water oxidation catalysts, lower than reported in two studies (at 640 and 750 mV)[12,26] but similar to two other studies done at comparable pH values (at 450 and 520 mV).[13,14] At first glance, it appears that the 2:1 ratio of 6,6′-dhbp to copper (in **1**) lowers the overpotential relative to the *in situ* prepared 1:1 ratio of the same components (with overpotential = 750 mV) described in the literature.[26] However, it is also worth noting that there may be an advantage to complexation of the copper(II) prior to dissolution in base, such as preventing formation of $Cu(OH)_2(s)$ and other insoluble salts. Small amounts of 2:1 complex could conceivably form in previously reported studies[26] and may perhaps be the active catalyst. Likewise, in our study changes may occur to the structure of **1** upon oxidation, which will be the subject of future investigations including computational studies.

DISCUSSION

Mechanistic Possibilities Suggested by Our Studies. The structures **1** are biomimetic[3] and show that 6,6′-dhbp can support a network of hydrogen bonds. This provides structural evidence that a high valent copper aqua or hydroxy species (formed from precatalyst **1**) could be stabilized by intramolecular hydrogen bonds. This has similarities to how enzymes use hydrogen bonds for O_2 activation and oxygen binding.[36−38] Hydrogen bonds have been shown computationally to facilitate dioxygen activation,[39] and dioxygen activation is the microscopic reverse of water oxidation.

Our evidence (Figure 10) presented herein supports that precatalyst **1** acts through a mononuclear species. However, **1** is a sluggish catalyst (as are *in situ* prepared 1:1 6,6′-dhbp Cu catalysts[26]). In our case with **1**, O−O bond formation may be the rate-limiting step. Similarly, with ruthenium catalysts O−O bond formation is often the rate-limiting step, and binuclear catalysts have allowed for faster rates.[40]

Lastly, pyridinol rings are also potentially redox noninnocent,[21,26] and this is a biomimetic strategy[41] for performing multielectron reactions with first row transition metals.[42] Thus, these combined 6,6′-dhbp ligand features can facilitate PCET and stabilize key intermediates. This provides a reasonable working hypothesis for the relatively low overpotentials observed.

CONCLUSIONS

The well-characterized 2:1 complex of $[(6,6'\text{-dhbp})_2Cu]^{2+}$ (**1a**) has four acidic protons, and upon removal of these protons with aqueous base, electrocatalytic water oxidation is observed. It is likely that proximal O^-/OH groups play a role in shuttling protons and stabilizing proposed high valent copper oxo species, perhaps similarly to the oxygen evolving complex in photosystem II.[2] Furthermore, the crystal structures described herein support the idea that hydrogen bonding interactions observed with 6,6′-dhbp facilitate transformations of the water substrate. Additionally, our prior work[21] showed that 6,6′-dhbp is a noninnocent ligand, and therefore perhaps can mimic the role of tyrosine in photosystem II by accelerating PCET events. While the low overpotential (477 mV) observed for **1** is impressive, the turnover rate was slow (0.356 s^{-1}) and may reflect slow O−O coupling. This work serves to illustrate what productive (water oxidation) and nonproductive pathways (competing irreversible oxidation to form a side product) are available to copper complexes of 6,6′-dhbp in basic aqueous solution under electrocatalytic conditions.

EXPERIMENTAL SECTION

General. The syntheses of 6,6′-dhbp, 6,6′-dmbp, and 4,4′-dhbp were adapted from the literature.[43,44] All other chemicals were procured from commercial sources. A Fisher Scientific "accumet" glass electrode was used to measure pH values and was calibrated with standard buffer solutions. Electronic absorption spectra were recorded with a PerkinElmer Lamda 35 spectrophotometer. Electrochemical

dx.doi.org/10.1021/ic501018a | *Inorg. Chem.* 2014, 53, 12689−12698

studies were performed on a CHI760C potentiostat. Additional synthetic schemes, catalytic tables and plots, spectroscopic data, and X-ray single crystal diffraction studies are provided in the Supporting Information. Elemental analyses were performed by Atlantic Microlab, Inc., Norcross, GA.

Acidity Studies. The pK_a studies of solutions of complex **2** were performed using concentrated solutions of NaOH and HCl to adjust the pH with neglibible change in volume. The pH was monitored before and after the solution absorption measurements.

EPR and ENDOR Spectroscopy. CW EPR spectra were measured on a Bruker ELEXSYS E540 X-band spectrometer with an ER 4102 ST resonator. CW spectra were measured at a microwave frequency of 9.44 GHz with 2.104 mW of power using 100 kHz magnetic field modulation with an amplitude of 2.00 mT. Aqueous samples of 2 mM of **1** at pH values ranging from 3.5 to 13.3 were mixed with 10% ethylene glycol and frozen at 77 K for spectra acquisition. Spectra were simulated on Matlab using Easyspin (see the Supporting Information (SI) for spectra, fits, g and A values).[45] Pulsed X-band ENDOR experiments were made with a Bruker ELEXSYS E-680W/X EPR spectrometer in an EN 4118X-MD4-W1 resonator in a Flexline cryostat with an ENI A-500 RF power amplifier using the Mims ENDOR ($(\pi/2)-\tau-(\pi/2)-T-(\pi/2)-\tau-$echo) pulse sequence with a 10 μs RF π-pulse applied during the delay time T with τ set at 128 ns. ENDOR experiments were ran at 50 K at three different pH values ranging from 8 to 13.3 for nitrogen interaction with the paramagnetic copper center.

HYSCORE Spectroscopy. Pulsed EPR measurements were made at 50 K with a nominal frequency of 9.77 GHz at different pH values to examine ligands within 0.5 nm of the copper center in frozen solutions of complex **1**. An ELEXSYS E680 EPR spectrometer (Bruker-Biospin, Billerica, MA) equipped with a Flexline ER 4118 CF cryostat and ER 4118X-MD4 ENDOR resonator was used to carry out pulsed measurements. HYSCORE uses a four pulse microwave sequence $(\pi/2)-\tau-(\pi/2)-t_1-\pi-t_2-(\pi/2)-\tau-$echo repeated at a rate of 2 kHz where $(\pi/2)$ and π indicate microwave pulses with nominal widths of 16 and 32 ns, respectively, that rotate the spins by that angle. The time between the first two pulses, τ, was optimized for proton and ^{13}C detection at 124 ns.[34] The times, t_1 and t_2, after the second and third pulse were incremented independently and generate the two axes of the HYSCORE spectrum. Cross-peaks in the spectrum correlate ENDOR frequencies for the two different values of the electron spin. HYSCORE measurements were taken at pH = 6.2, 10.0, 11.0, 12.5, and 13.3.

Water Oxidation Studies. A 0.1 M NaOAc/NaOH solution adjusted to the appropriate pH with either NaOAc or NaOH was used as the electrolyte in all studies. Specific details are included when discussed for each experiment. The glassy carbon working electrode had a disk surface area of 0.28 cm^2, and the Pt counter electrode had a disk surface area of 0.08 cm^2. The reference electrode used for the aqueous electrochemistry was aqueous Ag/AgCl/saturated KCl porous Teflon tip. The reference electrode used for nonaqueous electrochemistry was a AgCl coated Ag wire calibrated against $FeCp_2$/$FeCp_2^+$. CV data fitting was done by using a DigiElch electrochemical simulation software (DigiElch 7) for a ECC reaction.

Synthesis of [(6,6′-dhbp)$_2$Cu]SO$_4$ (1 as 1a and 1c). Copper(II) sulfate pentahydrate (0.133 g, 0.53 mmol) and 6,6′-dhbp (0.200 g, 1.06 mmol) were heated at 160 °C in 10 mL of ethylene glycol for 15 h. The solvent was then reduced and taken up in a 1:1 mixture of CH_2Cl_2/CH_3OH and filtered to obtain 185 mg of the products (**1a** and **1c**). Crystals were obtained by slow evaporation from methanol. IR (ATR): ν(cm^{-1}) = 3109 [b, ν(O−H)], 2764 [m, ν(C−H, Ar)], 1603 [s, ν(C−N, Ar)], 1482 [s, ν(C−N, Ar)]. EPR (X-band 9.7 GHz) $g_{\|}$ = 2.345 ($A_{\|}$ = 168 gauss due to Cu, $I = {}^3/_2$), $g_{\perp}$ = 2.122. MS (FAB): m/z = 436.1 is consistent with [**1c** − H]$^+$ = [$C_{20}H_{13}N_4O_4Cu$]$^+$ (expected m/z = 436.02); all peaks showed the expected isotopic pattern. Anal. Calcd (%) for $C_{20}H_{16}O_8N_4SCu$ (solvent free **1a**): C, 44.82; H, 3.01; N, 10.46; S, 5.98. Found: C, 44.25; H, 3.40; N, 9.82; S, 4.48 (analysis is off relative to calculated **1a**, but is consistent with some *in situ* deprotonation of **1a** to form **1c** as observed crystallographically; also some coordinated water may be present).

Synthesis of [(4,4′-dhbp)$_2$Cu]SO$_4$ (2). 4,4′-dhbp was used in the synthesis described for **1** to obtain the product in 82% yield. IR (ATR): ν(cm^{-1}) = 3069 [b, ν(O−H)], 2535 [m, ν(C−H, Ar)], 1624 [s, ν(C−N, Ar)], 1463 [s, ν(C−N, Ar)]. Anal. Calcd (%) for $C_{20}H_{16}O_8N_4SCu$: C, 44.82; H, 3.01; N, 10.46; S, 5.98. Found: C, 44.39; H, 3.02; N, 10.23; S, 5.86.

Synthesis of [(6,6′-dmbp)$_2$Cu(NO$_3$)]$_2$[Cu(NO$_3$)$_4$] (3). Copper(II) nitrate hemi(pentahydrate) (0.322 g, 1.38 mmol) and 6,6′-dmbp (0.100 g, 0.462 mmol) were stirred in 20 mL of a 1:3 dichloromethane/methanol solution for 24 h. The solvent was removed under vacuum to obtain the product in 20% yield after recrystallization (66 mg, 0.046 mmol). Crystals were obtained by slow diffusion of diethyl ether into a methanol solution of the complex. HRMS (FAB) showed peaks at m/z = 279.0, 341.0, and 496 (weak) which indicate the fragments [(6,6′-dmbp)Cu]$^+$, [(6,6′-dmbp)Cu(NO$_3$)]$^+$, and [(6,6′-dmbp)$_2$Cu]$^+$, respectively.

Synthesis of [(6,6′-dmbp)Cu(SO$_4$)MeOH] (4). Copper(II) sulfate pentahydrate (33.5 mg, 0.13 mmol) and 6,6′-dmbp (58 mg, 0.27 mmol) were heated at 80 °C in 20 mL of methanol for 15 h. The reaction was evaporated to dryness to obtain the crude product. Crystals were obtained by slow evaporation from methanol to isolate recrystallized **4** in 75% yield. IR (ATR): ν(cm^{-1}) = 3109 [b, ν(O−H)], 2764 [m, ν(C−H, Ar)], 1603 [s, ν(C−N, Ar)], 1482 [s, ν(C−N, Ar)]. HRMS (LIFDI): m/z = 279.0183 [**4** − SO$_4$]$^+$ = [$C_{12}H_{12}N_2O_2Cu$]$^+$ (expected m/z = 279.0195 all peaks showed the expected isotopic pattern). Anal. Calcd (%) for $C_{12}H_{12}O_2N_2CuSO_4CH_3OH$: C, 38.29; H, 3.95; N, 6.87. Found: C, 39.77; H, 4.48; N, 7.21 (analysis is off relative to calculated **4**, but is consistent with the presence of residual solvent).

Synthesis of [(6,6′-dhbp)$_2$Zn](ClO$_4$)$_2$ (5). Zinc(II) perchlorate hexahydrate (197 mg, 0.53 mmol) and 6,6′-dhbp (200 mg, 1.06 mmol) were stirred in 30 mL of deionized water for 3 days. The reaction was evaporated to dryness and the product dissolved in acetonitrile and filtered to remove unreacted starting material. The solution was evaporated to dryness to obtain the crude product in 98% yield. Crystals were obtained in 1 week by slow diffusion of hexanes into acetonitrile to obtain the product in 29% yield. ^{1}H NMR (DMSO, 500 MHz, δ in ppm): 6.59 (s, 1H, H−Ar), 7.27 (s, 1H, H−Ar), 7.69 (s, 1H, H−Ar), 11.04 (s, 1H, H−O). IR (ATR): ν(cm^{-1}) = 3180.22 [b, ν(O−H)], 3000 [m, ν(C−H, Ar)], 1602 [s, ν(C−N, Ar)], 1590 [s, ν(C−N, Ar)]. MS (FAB): m/z = 439.0 [M − 2H]$^+$ = [$C_{20}H_{15}N_4O_4Zn$]$^+$ (expected m/z = 439.04), all peaks showed the expected isotopic pattern. Anal. Calcd (%) for $C_{20}H_{14}O_4N_4Zn$ (deprotonated **5**): C, 54.63; H, 3.21; N, 12.74. Found: C, 53.46; H, 3.57; N, 12.37 (analysis is off relative to calculated deprotonated **5**, but is consistent with the presence of some water and acetonitrile from the synthesis).

■ ASSOCIATED CONTENT

Ⓢ Supporting Information

Further experimental details for the synthesis, characterization, and electrochemical water oxidation studies where available on **1**, **2**, **3**, **4**, and **5**. Crystallographic information in CIF format. This material is available free of charge via the Internet at http://pubs.acs.org. The atomic coordinates for these structures have also been deposited with the Cambridge Crystallographic Data Centre as CCDC 1000450−1000455. The coordinates can be obtained, upon request, from the Director, Cambridge Crystallographic Data Centre, 12 Union Road, Cambridge CB2 1EZ, U.K.

■ AUTHOR INFORMATION

Corresponding Author

*E-mail: elizabeth.t.papish@ua.edu.

Author Contributions

‖The first two authors contributed equally to this work.

Notes

The authors declare no competing financial interest.

■ ACKNOWLEDGMENTS

We thank NSF CAREER (Grant CHE-0846383 and CHE-1360802 to E.T.P. and her group); NSF (Grant CHE-1153120 to S.P.); Drexel University; and the University of Alabama for generous financial support. The diffractometer (used by M.Z.) was funded by NSF Grant 0087210, by Ohio Board of Regents Grant CAP-491, and by Youngstown State University. We also thank Tim Wade (Drexel University), Qiaoli Liang (the University of Alabama), and Stephen Chan (University of Delaware LIFDI facility funded by NSF MIR CHE-1229234) for MS analysis; Matthew Krzyaniak for EPR analysis; and Jared Paul for helpful discussions. A Drexel University Career Development award funded travel to seminars and conferences to discuss this project with colleagues. Finally, we thank the members of the Papish group for assistance and suggestions.

■ REFERENCES

(1) Lewis, N. S.; Nocera, D. G. *Proc. Natl. Acad. Sci. U.S.A.* **2006**, *103*, 15729.
(2) Umena, Y.; Kawakami, K.; Shen, J.-R.; Kamiya, N. *Nature* **2011**, *473*, 55.
(3) Bertini, I.; Gray, H. B.; Stiefel, E. I.; Valentine, J. S. *Biological Inorganic Chemistry*; University Science Books: Sausalito, CA, 2007.
(4) Concepcion, J. J.; Jurss, J. W.; Brennaman, M. K.; Hoertz, P. G.; Patrocinio, A. O. T.; Murakami, I. N. Y.; Templeton, J. L.; Meyer, T. J. *Acc. Chem. Res.* **2009**, *42*, 1954.
(5) Blakemore, J. D.; Schley, N. D.; Balcells, D.; Hull, J. F.; Olack, G. W.; Incarvito, C. D.; Eisenstein, O.; Brudvig, G. W.; Crabtree, R. H. *J. Am. Chem. Soc.* **2010**, *132*, 16017.
(6) McDaniel, N. D.; Coughlin, F. J.; Tinker, L. L.; Bernhard, S. *J. Am. Chem. Soc.* **2008**, *130*, 210.
(7) Dismukes, G. C.; Brimblecombe, R.; Felton, G. A. N.; Pryadun, R. S.; Sheats, J. E.; Spiccia, L.; Swiegers, G. F. *Acc. Chem. Res.* **2009**, *42*, 1935.
(8) Fillol, J. L.; Codolà, Z.; Garcia-Bosch, I.; Gómez, L.; Pla, J. J.; Costas, M. *Nat. Chem.* **2011**, *3*, 807.
(9) McAlpin, J. G.; Stich, T. A.; Ohlin, C. A.; Surendranath, Y.; Nocera, D. G.; Casey, W. H.; Britt, R. D. *J. Am. Chem. Soc.* **2011**, *133*, 15444.
(10) Reece, S. Y.; Hamel, J. A.; Sung, K.; Jarvi, T. D.; Esswein, A. J.; Pijpers, J. J. H.; Nocera, D. G. *Science* **2011**, *334*, 645.
(11) Dinca, M.; Surendranath, Y.; Nocera, D. G. *Proc. Natl. Acad. Sci. U.S.A.* **2010**, *107*, 10337.
(12) Barnett, S. M.; Goldberg, K. I.; Mayer, J. M. *Nat. Chem.* **2012**, *4*, 498.
(13) Chen, Z.; Meyer, T. J. *Angew. Chem., Int. Ed.* **2012**, *52*, 700.
(14) Zhang, M.-T.; Chen, Z.; Kang, P.; Meyer, T. J. *J. Am. Chem. Soc.* **2013**, *135*, 2048.
(15) Coggins, M. K.; Zhang, M.-T.; Chen, Z.; Song, N.; Meyer, T. J. *Angew. Chem., Int. Ed.* **2014**, *53*, 12226.
(16) Privalov, T.; Åkermark, B.; Sun, L. *Chem.—Eur. J.* **2011**, *17*, 8313.
(17) Papish, E. T.; Nieto, I. Patent Application Filed with US Patent Office 2012, PCT/US2012/052518, Provisionally filed 8/30/11 and final application filed 8/27/12.
(18) Nieto, I.; Livings, M. S.; Sacci, J. B.; Reuther, L. E.; Zeller, M.; Papish, E. T. *Organometallics* **2011**, *30*, 6339.
(19) Conifer, C. M.; Law, D. J.; Sunley, G. J.; Haynes, A.; Wells, J. R.; White, A. J. P.; Britovsek, G. J. P. *Eur. J. Inorg. Chem.* **2011**, *2011*, 3511.
(20) Conifer, C. M.; Taylor, R. A.; Law, D. J.; Sunley, G. J.; White, A. J. P.; Britovsek, G. J. P. *Dalton Trans.* **2011**, *40*, 1031.
(21) DePasquale, J.; Nieto, I.; Reuther, L. E.; Herbst-Gervasoni, C. J.; Paul, J. J.; Mochalin, V.; Zeller, M.; Thomas, C. M.; Addison, A. W.; Papish, E. T. *Inorg. Chem.* **2013**, *52*, 9175.
(22) Marelius, D. C.; Bhagan, S.; Charboneau, D. J.; Schroeder, K. M.; Kamdar, J. M.; McGettigan, A. R.; Freeman, B. J.; Moore, C. E.; Rheingold, A. L.; Cooksy, A. L.; Smith, D. K.; Paul, J. J.; Papish, E. T.; Grotjahn, D. B. *Eur. J. Inorg. Chem.* **2014**, 676.
(23) Hufziger, K. T.; Thowfeik, F. S.; Charboneau, D. J. N. I.; Dougherty, W. G.; Kassel, W. S.; Dudley, T. J.; Merino, E. J.; Papish, E. T.; Paul, J. J. *J. Inorg. Biochem.* **2014**, *130*, 103.
(24) Kawahara, R.; Fujita, K.-i.; Yamaguchi, R. *J. Am. Chem. Soc.* **2012**, *134*, 3643.
(25) Wang, W.-H.; Hull, J. F.; Muckerman, J. T.; Fujita, E.; Himeda, Y. *Energy Environ. Sci.* **2012**, *5*, 7923.
(26) Zhang, T.; Wang, C.; Liu, S.; Wang, J.-L.; Lin, W. *J. Am. Chem. Soc.* **2014**, *136*, 273.
(27) Addison, A. W.; Rao, T. N.; Reedijk, J.; Rijn, J. v.; Verschoor, G. C. *J. Chem. Soc., Dalton Trans.* **1984**, 1349.
(28) Klein, S.; Dougherty, W. G.; Kassel, W. S.; Dudley, T. J.; Paul, J. J. *Inorg. Chem.* **2011**, *50*, 2754.
(29) Kimblin, C.; Murphy, V. J.; Hascall, T.; Bridgewater, B. M.; Bonanno, J. B.; Parkin, G. *Inorg. Chem.* **2000**, *39*, 967.
(30) Su, C.-Y.; Liao, S.; Wanner, M.; Fiedler, J.; Zhang, C.; Kang, B.-S.; Kaim, W. *Dalton Trans.* **2003**, 189.
(31) Garribba, E.; Micera, G.; Sanna, D.; Strinna-Erre, L. *Inorg. Chim. Acta* **2000**, *299*, 253.
(32) Conner, K. P.; Schimpf, A. M.; Cruce, A. A.; McLean, K. J.; Munro, A. W.; Frank, D. J.; Krzyaniak, M. D.; Ortiz de Montellano, P.; Bowman, M. K.; Atkins, W. M. *Biochemistry* **2014**, *53*, 1428.
(33) Conner, K. P.; Vennam, P.; Woods, C. M.; Krzyaniak, M. D.; Bowman, M. K.; Atkins, W. M. *Biochemistry* **2012**, *51*, 6441.
(34) Hofer, P. *J. Magn. Reson., Ser. A* **1994**, *111*, 77.
(35) Concepcion, J. J.; Binstead, R. A.; Alibabaei, L.; Meyer, T. J. *Inorg. Chem.* **2013**, *52*, 10744.
(36) Ozaki, S.-i.; Roach, M. P.; Matsui, T.; Watanabe, Y. *Acc. Chem. Res.* **2001**, *34*, 818.
(37) Sahu, S.; Widger, L. R.; Quesne, M. G.; de Visser, S. P.; Matsumura, H.; Moënne-Loccoz, P.; Siegler, M. A.; Goldberg, D. P. *J. Am. Chem. Soc.* **2013**, *135*, 10590.
(38) Yang, J.; Kloek, A. P.; Goldberg, D. E.; Mathews, F. S. *Proc. Natl. Acad. Sci. U.S.A.* **1995**, *92*, 4224.
(39) Aullón, G.; Gorun, S. M.; Alvarez, S. *Inorg. Chem.* **2006**, *45*, 3594.
(40) Muckerman, J. T.; Polyansky, D. E.; Wada, T.; Tanaka, K.; Fujita, E. *Inorg. Chem.* **2008**, *47*, 1787.
(41) Gagliardi, C. J.; Vannucci, A. K.; Concepcion, J. J.; Chen, Z.; Meyer, T. J. *Energy Environ. Sci.* **2012**, *5*, 7704.
(42) Chirik, P. J.; Wieghardt, K. *Science* **2010**, *327*, 794.
(43) Dubreuil, D. M.; Pipelier, M. G.; Pradere, J. P.; Bakkali, H.; Lepape, P.; Delaunay, T.; Tabatchnik, A. PCT Int. Appl. 2008; WO2008012440.
(44) Himeda, Y.; Onozawa-Komatsuzaki, N.; Sugihara, H.; Kasuga, K. *Organometallics* **2007**, *26*, 702.
(45) Stoll, S.; Schweiger, A. *J. Magn. Reson.* **2006**, *178*, 42.